Diffusion Controlled Synthesis of PbS and PbSe Quantum Dots with In-Situ Halide Passivation for Quantum Dot Solar Cells.

ARTICLE *in* ACS NANO · DECEMBER 2013

Impact Factor: 12.88 · DOI: 10.1021/nn405236k · Source: PubMed

5 AUTHORS, INCLUDING:

Elisa M Miller
University of Colorado Boulder
22 PUBLICATIONS **200** CITATIONS
SEE PROFILE

Joseph M Luther
National Renewable Energy Laboratory
83 PUBLICATIONS **5,246** CITATIONS
SEE PROFILE

Matthew C Beard
National Renewable Energy Laboratory
114 PUBLICATIONS **7,873** CITATIONS
SEE PROFILE

Diffusion-Controlled Synthesis of PbS and PbSe Quantum Dots with *in Situ* Halide Passivation for Quantum Dot Solar Cells

Jianbing Zhang,[†,§] Jianbo Gao,[‡,§] Elisa M. Miller,[‡] Joseph M. Luther,[‡] and Matthew C. Beard[‡,*]

[†]School of Optical and Electronic Information, Huazhong University of Science and Technology, 1037 Luoyu Road, Wuhan, Hubei 430074, China and [‡]Chemical and Material Sciences Center, National Renewable Energy Laboratory, 1617 Cole Boulevard, Golden, Colorado 80401, United States. [§]J. Zhang and J. Gao contributed equally to this work.

ABSTRACT

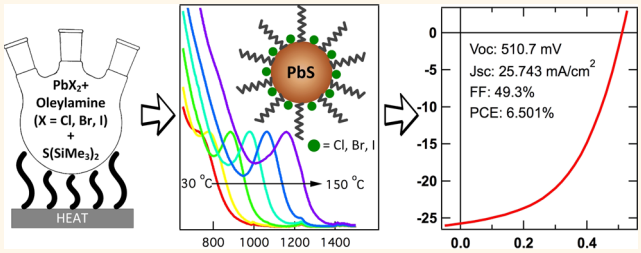

We developed a simple non-hot-injection synthetic route that achieves *in situ* halide-passivated PbS and PbSe quantum dots (QDs) and simplifies the fabrication of Pb-chalcogenide QD solar cells. The synthesis mechanism follows a temperature-dependent diffusion growth model leading to strategies that can achieve narrow size distributions for a range of sizes. We show that PbS QDs can be produced with a diameter as small as 2.2 nm, corresponding to a 1.7 eV band gap, while the resulting size distribution (6−7%) is comparable to that of hot-injection syntheses. The *in situ* chloride surface passivation is demonstrated by X-ray photoelectron spectroscopy and an improved photostability of both PbS and PbSe QDs when stored under air. Additionally, the photoluminescence quantum yield of the PbS QDs is ∼30% higher compared to the traditional synthesis. We show that PbS QD solar cells with 6.5% power conversion efficiency (PCE) can be constructed. Finally, we fabricated PbSe QD solar cells in air (rather than in inert atmosphere), achieving a PCE of 2.65% using relatively large QDs with a corresponding band gap of 0.89 eV.

KEYWORDS: halide passivation · lead sulfide · lead selenide · colloidal quantum dot · quantum dot solar cell

PbS and PbSe quantum dots (QDs) are being investigated for use in solar cells[1−5] and photodetectors[6,7] due to strong quantum confinement,[8] ease of synthesis,[9,10] and beneficial quantum-confinement effects, such as multiple exciton generation.[11−13] In the most common implementation, the QDs are employed in thin films (QD solids) where the QDs are electronically coupled to one another and the emergent macroscopic optoelectronic properties define device performance. Charge-carrier transport within QD solids is determined by both the degree of QD−QD electronic coupling and shallow and midgap defect states generally associated with disorder[14,15] and imperfect QD surfaces. Current approaches to QD-film formation use various chemical reagents to treat the QDs in a layer-by-layer fashion to form smooth but disordered QD arrays.[16] These chemical reagents are generally chosen to reduce the QD−QD spacing by exchanging the long aliphatic as-synthesized surface ligands[16,17] with smaller compact ligands. However, transport properties have also shown a dependence on the chemical nature of the ligand−surface or ligand−QD interaction. Furthermore, the chemical reagents can induce a variety of phenomena in QD solutions and arrays that are only beginning to be understood, such as QD−QD fusion,[18] QD−QD alignment,[19] passivation of surface dangling bonds, or creation of surface defects.

* Address correspondence to matt.beard@nrel.gov.

Received for review October 7, 2013 and accepted December 16, 2013.

Published online December 16, 2013
10.1021/nn405236k

Recently, QD devices have benefited from multiple ligand moieties used in postsynthetic processing presumably to control or passivate different surface facets or different surface-related defect states. For example, PbS QD solar cells with power conversion efficiencies greater than 4.5% have typically employed secondary surface treatments.[3] Ip *et al*. demonstrated that halide anions can be employed postsynthetically to achieve a PbS QD solar cell with 7.0% efficiency.[2,20] Similarly, Semonin *et al*. employed a secondary hydrazine treatment to significantly improve the performance of PbSe QD-based solar cells,[1] and Gao *et al*. found that PbS QD solar cells benefit from secondary treatments.[3,21] Halide treatments are attractive because the resulting ligand is compact and in the case of chloride ions resistive toward oxidative attack.[22] Anion substitution within the Pb chalcogenide lattice can also be an effective strategy for n-doping of the QD film.[23]

Halide termination has been explored in several QD systems. Owen *et al*. developed ligand exchange reactions to produce chloride-terminated CdSe QDs.[24,25] The goal was to employ the chloride ion as a compact atomic ligand in QD solids, achieving minimal QD−QD separation. They also found that chloride ions can balance excess charge resulting from nonstoichiometric surface termination.[24,25] Zanella *et al*. introduced a ligand exchange reaction based upon propyl trichlorosilane similar to that of Owen *et al*. where the reaction replaces the native ligands with chloride termination but also tends to slightly etch the QDs.[26] Nevertheless, they demonstrated that such reactions are general for many QD systems and produce functional QD solids. Bae *et al*. exposed oleate-terminated PbSe QDs to chlorine gas and found that the chlorine gas reacts with PbSe QDs to produce chloride-terminated QDs.[22] The resulting QDs showed improved photoluminescence quantum yields (PLQYs) and photostability, which the authors suggest results from fewer exposed Se surfaces that are otherwise prone to oxidation.[22] Wheeler and co-workers recently explored the use of $SiCl_4$ in place of SiH_4 as a precursor gas for the hydrothermal plasma synthesis of Si QDs,[27] producing chloride-terminated Si QDs. The chloride termination allowed for a hypervalent interaction with polar solvents that leads to colloidal stability.[27] These studies demonstrate that QD surface chemistry is an active area of research and QD photophysics can benefit from halide termination.

Progress in implementing QDs in novel approaches to solar energy capture and usage relies on simple and reproducible procedures for QD-layer formation. Here we show that introducing the halide during the growth of the QDs (*in situ*) allows for improved surface passivation and a simplified device fabrication procedure. Synthetic approaches incorporating lead chloride precursors have been explored by Cademartiri *et al*.[28] and Moreels *et al*.,[29] who synthesized PbS QDs using $PbCl_2$ in oleylamine (OLA) and demonstrated higher PLQYs and better stability compared to the conventionally synthesized QDs using PbO as the precursor. With these methods, it is difficult to control the synthesis of the smaller PbS QDs, where the smallest QD sizes correspond to a first exciton peak of 1.34 eV.[30] However, it is desirable to obtain larger band gaps, which routinely lead to higher power conversion efficiencies for QD solar cells. Furthermore, PbS QDs are being actively pursued for solution-processed multijunction solar cells, and higher band-gap materials are necessary for their optimization. Therefore, it is desirable to develop syntheses with a broader size control that lead to better surface passivation without further secondary ligand exchange.

RESULTS AND DISCUSSION

In the previous $PbCl_2$ hot-injection syntheses,[28,29] sulfur dissolved in OLA is injected into the Pb precursor solution to form PbS QDs. This reaction scheme works well to produce larger QD sizes but is unable to achieve QDs with diameters smaller than ~3 nm due to a relatively low nucleation threshold with S:OLA. We tried a more reactive sulfur source commonly used in the PbS synthesis,[9] bis(trimethylsilyl) sulfide (TMS_2S), in order to obtain smaller PbS QDs. However, the hot-injection method resulted in a very broad size distribution when TMS_2S is used at higher temperature. Upon reducing the injection temperature, we find that a low-temperature reaction method is very suitable for this synthesis and can produce a wide range of various-sized PbS QDs with reasonable narrow size distributions. We demonstrate that the growth dynamics follow a diffusion-controlled growth model. We also explore the use of $PbBr_2$ and PbI_2 as the Pb precursor so as to produce bromide- or iodide-terminated QDs. We further extend this synthetic strategy to produce air-stable PbSe QDs. Our reaction can be classified as a "heat-up" synthesis rather than the more conventional hot-injection synthesis and as such should be amenable to large scale-up strategies.[31]

Specifically, PbX_2 (X = Cl, Br, or I) and OLA are combined and then heated between 100 and 140 °C and cooled to room temperature (30 °C). The mixture becomes gel-like during the cooling process, and the viscosity at 30 °C depends on the precursor, which varied according to $PbCl_2$ > $PbBr_2$ > PbI_2 (determined by eye). TMS_2S was added at 30 °C, and the temperature of the solution was increased under constant stirring. Once the final temperature is reached, the reaction is quenched using a water bath. The rate at which the temperature is raised minimally affects the final QD size, where a lower rate results in slightly larger sizes. Figure 1a−c show the evolution of the absorption spectra of the PbS QDs when the growth temperature is increased from 30 °C to various final temperatures (noted in Figure 1a) up to 150 °C using

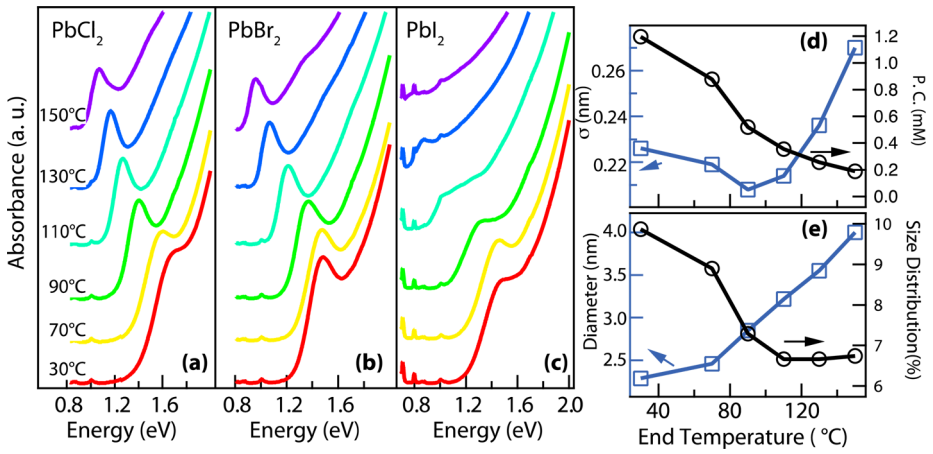

Figure 1. Evolution of absorption spectra of PbS QDs synthesized from (a) $PbCl_2$, (b) $PbBr_2$, and (c) PbI_2 as well as (d) particle concentration (P.C.), black trace, and standard deviation of the size distribution, blue trace, of the PbS QDs and (e) size of PbS QDs synthesized from $PbCl_2$, blue trace, and size distribution (%), black trace, during the growth temperature ramping process. The absorption features in the range 0.73−0.62 eV and other small sharp peaks are due to hydrocarbons present in the reaction solution.

$PbCl_2$, $PbBr_2$, or PbI_2, respectively. Since OLA is weakly bound to the QD surface,[32] we exchange the as-synthesized ligands to the conventional oleate ligand to improve their colloidal stability.[29] Further details can be found in the Methods section.

$PbCl_2$, $PbBr_2$, and PbI_2 each lead to varying growth dynamics due to differences in their viscosity and reactivity. The QDs grow as the temperature increases (Figure 1). Correspondingly, the size distribution narrows and saturates below 7% for final temperatures above 110 °C (Figure 1e, black trace for $PbCl_2$). We also plot the standard deviation, σ (Figure 1d, blue trace), of the size distribution and use that to evaluate the size-focusing growth. Using the relationship between the optical band gap (E_g) and QD diameter and the relationship between QD diameter and molar extinction coefficient at 400 nm,[29] we calculate the concentration of QDs (P.C.) formed at various temperatures during the synthesis. The error in determining the size distribution is dependent on the error of the sizing curve, where we have used literature reports.[29] (Any error in the sizing curve will produce a systematic error in our size determination but will not impact the conclusions of this work.) As the temperature increases, the number of QDs decreases (Figure 1d, black line). Higher temperatures lead to larger QDs, indicating the temperature is a driving force for growth. We also observe that PbX_2 and OLA form a turbid suspension rather than a clear solution, so the growth of the PbS QDs is in a heterogeneous system.[28] The above observations can be described by a diffusion- or mass-transport-controlled growth,[28,33] where the diffusion coefficient of the monomer affects the growth substantially.

Peng *et al.* and Talapin *et al.* have experimentally[34] and theoretically[33] shown that size focusing occurs when QDs grow in monomer oversaturation conditions and there is slow diffusion of monomers. "Monomer" here refers to the molecular or atomic units that add/dissolve to/from the surface of the QD, and we do not attempt to identify the monomer species. The growth in our synthesis is maintained by an increase in temperature and the corresponding increase of the diffusion coefficient. The diffusion coefficient depends on temperature and viscosity as described by Stokes−Einstein equation:

$$D = \frac{k_B T}{6\pi\eta r} \quad (1)$$

where k_B is Boltzman's constant, T is temperature, η is viscosity, and r is the particle radius. In this reaction, D is controlled by the viscosity and temperature, where the viscosity depends upon the precursor concentration and chemical identity, as noted above. Viscosity is also temperature-dependent (the higher the temperature, the lower the viscosity);[35] therefore the diffusion coefficient increases with temperature more than the linear dependence indicated in eq 1. Talapin *et al.* derived an equation that describes the growth rate, dr/dt, of a single QD,[33]

$$\frac{dr}{dt} = V_m D C_{flat}^{0} \left\{ \frac{S - \exp\left[\frac{2\gamma V_m}{rRT}\right]}{r + \frac{D}{k_g^{flat}} \exp\left[\alpha \frac{2\gamma V_m}{rRT}\right]} \right\} \quad (2)$$

where V_m is molar volume, D is the diffusion coefficient, C_{flat}^{0} is the solubility of the monomer in equilibrium with a flat interface, S describes the oversaturation (which is proportional to the amount of monomer remaining in the bulk solution relative to its equilibrium value), γ is the specific surface energy, R is the gas constant, T is temperature, r is the radius of a growing particle, k_g^{flat} is the growth rate constant for growth of a flat ($r = \infty$) surface, and α is a transfer coefficient.

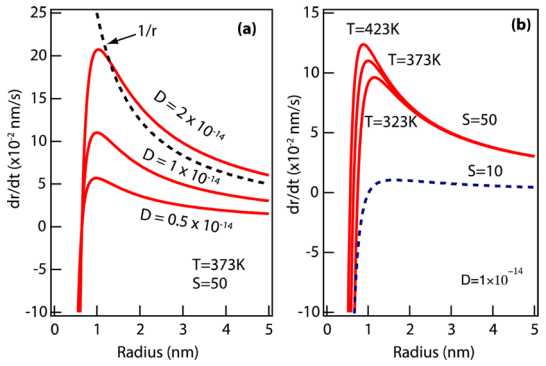

Figure 2. Growth rate (d*r*/d*t* where *r* is the radius) *vs* QD radius calculated from eq 2 for (a) different diffusion coefficients and (b) temperatures. The parameters are γ = 0.125 J/m^2, V_m = 3.15 × 10^{-5} m^3/mol (for PbS), C_{flat}^0 = 0.01 mol/m^3, α = 0.5, k_g^{flat} = 5.2 × 10^{-4} M/s. In part (b), k_g^{flat} and *D* are held constant; however, k_g^{flat} is temperature-dependent ($\propto$ exp(−1/*T*)) and *D* increases rapidly with temperature (see text). Therefore, the dependence of d*r*/d*t* on temperature will be greater than shown here. The dashed trace in (a) displays a 1/*r* dependence. The dashed blue trace in part (b) demonstrates that the 1/*r* dependence is reduced when the oversaturation conditions are reduced (here *T* = 423 K and *S* = 10).

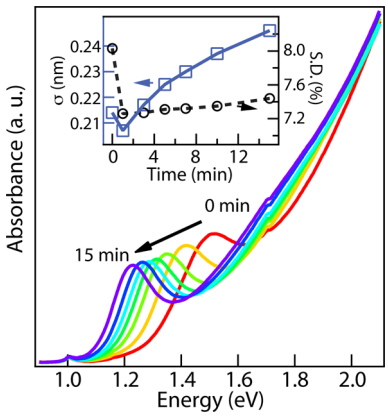

Figure 3. Evolution of absorption spectra during growth of PbS QDs with $PbCl_2$ precursor and maintaining the temperature at 80 °C for 15 min. The inset shows the evolution of the standard deviation and size distribution.

In Figure 2, we plot d*r*/d*t* for various values of *D* (Figure 2a) and temperature (Figure 2b) to demonstrate that the growth rate increases with both diffusion coefficient and temperature. When *D* is small and *S* (oversaturation) is large, the growth rate of individual QDs varies as 1/*r* (Figure 2a dashed black trace) so that larger QDs grow slower than smaller QDs and the ensemble size distribution focuses. When the temperature is low, the growth rate is small due to both a lower temperature and smaller diffusion coefficient (higher viscosity). Thus, it takes longer to consume monomers and reduce the oversaturation condition. Figure 2b compares conditions at *T* = 423 K for *S* = 50 and 10 (dashed blue trace) and demonstrates that the 1/*r* conditions are decreased when the oversaturation is reduced. We demonstrate these features by monitoring the evolution of size distribution when the temperature is maintained at 80 °C for 15 min (see Figure 3). It takes approximately 3 min to reduce the oversaturation conditions and thus reverse the size focusing (inset of Figure 3, blue squares). The synthesis conducted by Cademartiri *et al.*[28] also confirms slow consumption of monomers due to a slow growth rate controlled by monomer diffusion. In their study, a stable narrow size distribution evolves from an initial broad distribution in more than 20 min when the $PbCl_2$ concentration is high; in this case, the slower diffusion occurs because of a higher viscosity. By employing a lower $PbCl_2$ concentration, the growth reached a stationary regime faster.

As the temperature increases during synthesis, the diffusion coefficient increases, resulting in a greater growth rate. When the temperature is low, the growth rate is too small to reduce the oversaturation during the initial temperature increase, leading to a high oversaturation condition. As a result, the size distribution narrows as shown in Figure 1e (30−110 °C). Higher temperatures lead to higher *D* and thus a larger difference of growth rates between small and large QDs and thus to a larger degree of size focusing. The dissolution of QDs that are smaller than the critical radius, r_{cr}, also contributes to maintaining the oversaturation conditions by releasing monomers, where $r_{cr} = 2\gamma V_m/RT \ln S$ when d*r*/d*t* = 0 (eq 2).[33,36] We show that the size distribution can be tuned by manipulating the oversaturation conditions during growth. We withdrew one-third of the reaction solution at 30 °C immediately after injection of the sulfur precursor at 30 °C and then reinjected that aliquot back into the reaction flask when the temperature reached 115 °C. The reaction solution at 30 °C consisted of smaller QDs with a higher concentration and unreacted monomer; thus, we expect the particle concentration to increase after the addition of the aliquot. However, the particle concentration at 130 °C is smaller than that at 110 °C (see Figure 4a), indicating that most of the reinjected particles dissolve, as they are smaller than the critical size at 115 °C, leading to a delayed defocusing of the size distribution (see Figure 4b). These principles could be further employed to achieve narrow size distributions for any desired QD size.

We also study the effect of $PbCl_2$ concentration, which affects the growth rate through both the oversaturation conditions and solution viscosity. The QDs synthesized in different amounts of OLA reach approximately the same size during growth (Figure 4c), which results from similar overall growth rates. As discussed above, the growth rate increases with higher oversaturation of monomers and a higher diffusion coefficient. A greater $PbCl_2$ concentration leads to a higher oversaturation but a lower diffusion coefficient; these two conditions cancel one another, producing similar growth rates (Figure S3). However, the size deviation is

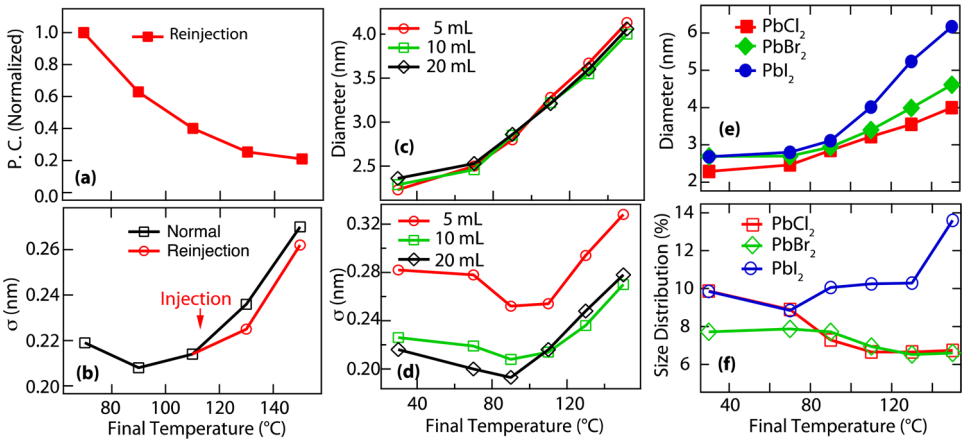

Figure 4. Evolutions of the size deviation and particle concentration of the PbS QDs when one-third of the reaction solution formed at 30 °C is reinjected at 115 °C. (a) Particle concentration for the test case where the solution is reinjected at 115 °C, demonstrating that the small QDs are redissolved at the higher temperature to increase the oversaturation conditions. (b) Comparison of the evolution of the size deviation of the normal synthesis to the reinjection synthesis. (c and d) Evolutions of average particle diameter and size deviation for the reaction using three $PbCl_2$ concentration conditions (different amounts of OLA). (e) Particle diameter for the different Pb-halide precursors at similar concentrations. (f) Comparison of the evolution of the size deviation.

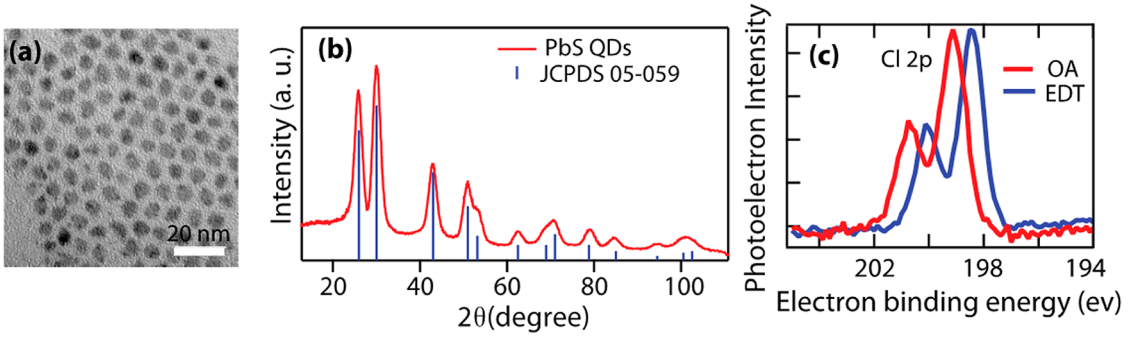

Figure 5. (a) Representative TEM of typical PbS QDs showing that the QDs remain quasi-spherical. (b) Comparison of the measured XRD to the PbS standard, confirming crystalline rock salt PbS. (c) XPS data for PbS QD films synthesized with $PbCl_2$ as-cast with oleate ligands (red trace) and synthesized with $PbCl_2$ and ligand exchanged with EDT (blue trace). The shift in the peak position and change in width between the red and blue traces are due to charging in the nonconductive oleate-capped QDs. The binding energy of the Cl 2p peak in the EDT-treated films is 198.4 eV and is consistent with a chloride bonding environment.[22,26]

markedly different for the three concentration conditions (Figure 4d). As the temperature increases, the size distribution focuses for each concentration. The initial size distribution is larger for the higher $PbCl_2$ concentration but undergoes more focusing; both effects can be attributed to the lower diffusion coefficient.

The growth of PbS QDs using $PbBr_2$ and PbI_2 further confirms the diffusion-controlled model. Due to a lower viscosity, the reaction solution has a higher diffusion coefficient ($D_{PbI_2} > D_{PbBr_2} > D_{PbCl_2}$). As a result, the PbS QDs synthesized from $PbBr_2$ form a narrow peak even at 30 °C due to faster diffusion (Figure 1b and Figure 4f). For the case of PbI_2, the diffusion is even faster such that the oversaturation conditions cannot be maintained, and the growth approaches the reaction-controlled regime where the size distribution is larger and defocuses (Figure 1c and 4f). Furthermore, visible metal particles (which are assumed to be lead) were formed when the PbI_2 and OLA mixture was heated to a higher temperature, likely resulting in less Pb precursor available. As a result, the QDs synthesized by PbI_2 show a much shorter size-focusing regime.

As discussed above, an advantage of this synthesis is the simple, *in situ* halide passivation and control of QD size. In Figure 5a, we show the TEM of a typical PbS synthesis demonstrating that the particles remain quasi-spherical. Figure 5b displays the XRD, confirming the synthesis produces crystalline PbS QDs, and Figure 5c shows the XPS of Cl 2p, confirming that chloride is retained in the PbS QDs. We checked that chloride survives after 1,2-ethanedithiol (EDT) treatment (Figure 5c, blue trace). The QD samples used for the measurements in Figure 5c consisted of dip-coated PbS QDs on an ITO substrate. Note, the peak is shifted and narrower than the Cl 2p peak from the as-produced PbS QDs (Figure 5c, red trace). This is due to charging effects[22,26] from the insulating ligands on the as-produced samples. The QD layers with EDT-exchanged ligands (Figure 5, blue trance) are conductive, and the peak position is 198.4 eV, consistent with a

Pb−Cl bond.[22,26] We measured the Pb:Cl ratio for ~3 nm PbS QDs of ~2.4 (Figure S4a), consistent with previously reported values[29] and indicating that the precursor has an effect on the final chemical composition of the QDs. The Pb:Cl ratio remains roughly constant before and after EDT treatment, while the Pb:S ratio decreases due to the addition of EDT to the QD surface (Figure S4).

One advantage of the diffusion-controlled synthesis presented here is that scaling up the reaction should in principle be more straightforward than the hot-injection synthesis. To demonstrate the feasibility of scaling our reaction, we produced a 7.4 g batch and a 47 g batch of PbS QDs (Figure 6). To achieve the 7.4 g sample, 8.34 g (30 mmol) of $PbCl_2$ and 80 mL of OLA are mixed with 2.1 mL (10 mmol) of TMS_2S diluted in 10 mL of OLA at 30 °C. The temperature was increased to 85 °C and maintained for 5 min. The final weight of the product contains PbS and ligand; therefore, we calculate the weight percent from the XPS data (Supporting Information) to be 43% Pb, corresponding to 15.4 mmol of Pb. The sulfur content is about one-third the Pb content for these samples, and therefore, the reaction yield is ~50% for both Pb and S precursors. To produce 47 g of PbS QDs, we mixed 83.4 g of $PbCl_2$ (300 mmol) with 600 mL of OLA and added 21 mL (100 mmol) of TMS_2S diluted in 20 mL of OLA. The solution is then heated to 85 °C and maintained for 8 min. The resulting PbS QD powder was 47.07 g, which gives a slightly lower reaction yield. No attempts were made to maximize the yield.

The *in situ* chloride passivation improves the photoluminescence and photostability. In Figure 7a inset, we compare the PLQY for PbO- and $PbCl_2$-synthesized QDs and find a ~30% higher PLQY. In Figure 7a, we show how the absorption spectra evolve when the sample is stored in air over the course of one month for the $PbCl_2$- compared to the PbO-synthesized QDs. For the $PbCl_2$-synthesized QDs, the peak positions remain constant, while they gradually blue-shift for the PbO-synthesized QDs, indicating oxidation of the surface.

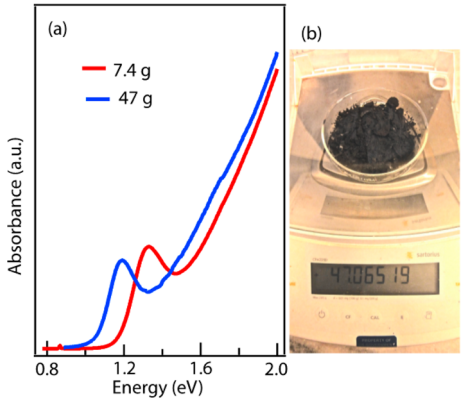

Figure 6. (a) Absorption spectra of the 7.4 and 47 g PbS scaled synthesis. (b) Picture of the 47 g PbS QD batch.

We successfully extended the synthesis scheme to PbSe QDs (Figure 7b) using $PbCl_2$ as the precursor; however in this case, we find that two selenium precursors with different reactivities are needed. Bis(trimethylsilyl) selenide (TMS_2Se), which is highly reactive, was used to form small QDs, and a relatively lower reactive precursor, TBPSe (selenium dissolved in tributylphosphine), was employed to maintain the oversaturation condition during the diffusion-controlled growth. When only TMS_2Se was used as the selenium precursor, the PbSe QDs grew but did not exhibit size focusing as the temperature increased (Figure S5) because the reactivity governs growth. Generally, PbSe QDs synthesized using PbO precursor exhibit instability under air exposure. This instability is due to the destructive oxidation and kinetically collision-induced decomposition, resulting in significant absorption and PL degradation.[37] Researchers have found that larger size PbSe QDs are more sensitive to oxygen and light compared to smaller size QDs presumably due to differences in facet reactivity with oxygen. The PbSe QDs synthesized with $PbCl_2$ have a first exciton peak at ~0.89 eV. These PbSe QDs show excellent stability when stored in air, and the initial PLQY of ~28% is stable over 30 days, only decreasing to 24% (see inset in Figure 7b). The *in situ* chloride passivation contributes to their stability, consistent with the PbS results and literature reports.[22]

Finally, we fabricated QD solar cells using the chloride-passivated PbS QDs, from QDs whose absorption spectrum is shown in Figure 7a, and compare to the conventionally synthesized PbS QDs. The architecture of the devices is ITO/ZnO/PbS(e) QDs/MoO_3/Al following our previous work.[3,21] The QD layer was fabricated by layer-by-layer dip coating in a fume hood using EDT to exchange the oleate ligand and form pinhole-free smooth films. The *J*−*V* characteristics of the various devices that we tested are shown in Figure 8, and their performance parameters are tabulated in Table 1.

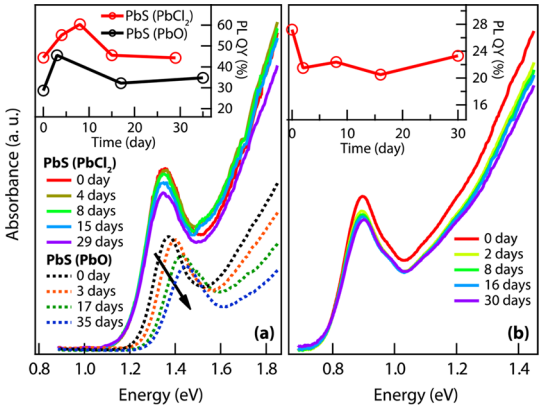

Figure 7. Evolution of absorption spectra and PLQY of (a) PbS QDs synthesized from $PbCl_2$ and PbO and (b) PbSe QDs synthesized from $PbCl_2$ when they were stored in tetrachloroethylene (TCE) in air. The circles in the insets represent ~5−8% error in the determination of the PLQY.

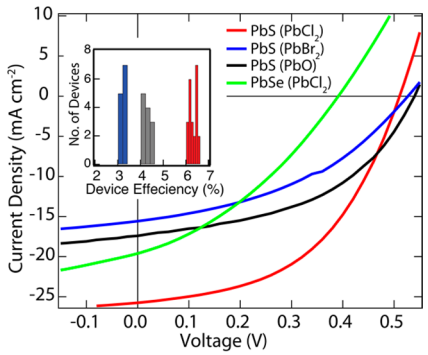

Figure 8. *J*–*V* characteristics of PbS or PbSe QD solar cells with an ITO/ZnO/PbS(e)/MoO_3/Al device. The PbS or PbSe QDs are synthesized with $PbCl_2$, $PbBr_2$, or PbO as lead precursors. Inset shows histograms of the device efficiencies for $PbCl_2$ (red bars), $PbBr_2$ (blue bars), and PbO (gray bars).

The PbS QDs synthesized from PbO and $PbBr_2$ were also used to fabricate solar cells, but the chloride-terminated PbS QDs showed better performance and achieved a power conversion efficiency of 6.5% (Figure 8, red trace). Device efficiencies greater than 4.5% could only be obtained using $PbCl_2$-derived QDs or further treatments of the PbO-derived QDs. The main improvement is an increase in the J_{sc} compared to the conventional devices. The bromide-terminated QDs did not exhibit better device performance (Figure 8, blue trace), which could be attributed to a weaker Pb–Br bond compared to the Pb–Cl bond. Supporting this hypothesis we find that bromide-terminated QDs are not as resistive toward oxidization as chloride-terminated QDs (Figure S6). We also fabricated PbSe QD solar cells, but in stark contrast to previous findings,[1] we are able to fabricate these devices in air similar to the PbS QD devices.[3,5,38] In past efforts, solar cells based on PbSe QDs could not be fabricated in air (devices did not show diode behavior), and air-free environments were employed. However, we show for the first time functional PbSe QD solar cells fabricated in air (Figure 8, green line). Here we used relatively large QDs (absorption spectrum shown in Figure 7b) that would typically undergo rapid oxidation in EDT-treated thin films.

TABLE 1. Device Performance Parameters for *J*–*V* Characteristics Shown in Figure 8

QD	J_{sc} (mA/cm^2)	V_{oc} (mV)	fill factor (%)	efficiency (%)
PbS($PbCl_2$)	25.743	510.7	49.3	6.501
PbS($PbBr_2$)	15.57	527.1	41.2	3.391
PbS(PbO)	17.38	540	47	4.405
PbSe($PbCl_2$)	19.6	391.3	34.8	2.653

CONCLUSIONS

In summary, *in situ* halide-passivated PbS QDs with a narrow size distribution can be attained using a non-hot-injection method. A temperature-dependent diffusion-controlled growth results in size focusing to produce a size distribution comparable to hot-injection synthetic routes. Small PbS QDs with a diameter as small as 2.2 nm, corresponding to a band gap of 1.7 eV, can be produced. The chloride-terminated QDs show improved stability in air and higher PLQY, demonstrating effective surface passivation, and the chloride is retained in EDT-treated films. The chloride-passivated PbS QDs exhibit much better solar cell performance compared to conventional synthesis, providing a simple way to construct highly efficient PbS colloidal QD solar cells. A working PbSe QD solar cell made in air was demonstrated for the first time, opening another avenue for further investigations.

METHODS

Materials. PbX_2 (X = Cl, Br, or I) (99.999%), oleylamine (OLA, tech. grade, 70%), bis(trimethylsilyl) sulfide (TMS_2S, synthesis grade), oleic acid (OA, tech. grade, 90%), selenium powder (99.99%), chloroform (anhydrous, 99+%), acetonitrile (anhydrous, 99.8%), tetrachloroethylene (TCE, ≥99.9%), hexane (≥95%), and ethanol (≥99.5%) were purchased from Aldrich. Tributylphosphine (TBP, tech. grade, ≥90%) and 1,2-ethanedithiol (EDT, purum ≥98.0%) were purchased from Fluka. Bis(trimethylsilyl) selenide (TMS_2Se) was purchased from Gelest. All the chemicals were used as received.

Synthesis of PbS QDs from Lead Halide. OLA (10 mL) and 3 mmol of PbX_2 (X = Cl, Br, or I) were degassed under vacuum at 80 °C, followed by heating to various temperatures (140 °C for $PbCl_2$ and $PbBr_2$, 100 °C for PbI_2) under nitrogen and maintained at these temperatures for 30 min. Then the suspension was allowed to cool to 30 °C, and 210 μL of TMS_2S dissolved in 2 mL of OLA was added to the flask (we have tried sulfur in OLA as the sulfur precursor, but it led to a broad size distribution). Next, the reaction solution was reheated to a higher temperature under vigorous stirring for the growth of the QDs. At various temperatures, 30 μL reaction solutions were withdrawn and quenched by 2.5 mL of TCE for the absorption measurements. Finally, a water bath was used to quench the QD growth when the desired size was achieved. The PbS QDs were separated from the raw solution by centrifugation after the addition of hexane and ethanol and then dissolved in hexane. OA (6 mL) was added to the purified QD solution to replace the weakly bound OLA, followed by storing for 24 h for the precipitation of unreacted PbX_2. The residual PbX_2 in the QD solution was removed by a 200 nm pore size filter. Finally, the PbS QDs were washed several times using hexane and ethanol. The washing process was performed in air. The PbS QDs synthesized from $PbBr_2$ lost stability in solvent after three washes. For the synthesis using PbI_2, metal particles (~3 mm in diameter, which are assumed to be lead) were formed when the PbI_2 and OLA mixture was heated to a higher temperature, likely resulting in less Pb precursor available throughout the reaction. As a result, the QDs synthesized by PbI_2 show a much shorter size-focusing regime (Figure 1c and Figure 4f). The I-terminated PbS QDs lost stability in solvents after only one wash.

Synthesis of PbSe QDs. $PbCl_2$ was used for the synthesis of PbSe QDs. The procedure is similar to that of PbS QDs with two exceptions: (1) TMS_2Se (0.5 mmol) and 0.67 mL of TBPSe (0.75 M) were added sequentially to the lead precursor at 30 °C; (2) the PbSe QDs were washed in a glovebox.

Study of Optical Stability of QDs. The QDs dissolved in TCE were stored in a 4 mL vial in air with the vial loosely capped.

At different times, the absorption spectra and PLQYs were measured.

Synthesis of ZnO Nanocrystals (NCs) and PbS QDs from PbO. ZnO NCs and PbS QDs from PbO were synthesized using our previous methods.[5,38]

Device Fabrication. The ZnO NCs solution (40 mg/mL in chloroform) was spin-coated at 2000 rpm for 1 min onto a cleaned glass substrate with prepatterned ITO electrodes in a fume hood. The resulting ZnO film was annealed on a hot plate set to 260 °C for 30 min to remove residual solvent. The PbS active layer was hand-dipped on the substrates in a fume hood under ambient atmosphere. The substrate was dipped into PbS/PbSe QDs in hexane (~10 mg/mL), carefully withdrawn by hand, allowed to dry, and then dipped into 1 mM EDT in acetonitrile. Thirty dip-coating cycles were performed to build up a layer of 200−270 nm on top of the ZnO film. The top electrode was deposited by thermal evaporation, consisting of 15 nm molybdenum trioxide at a rate of 0.5 Å s^{-1} and 150 nm aluminum at a rate of 20 Å s^{-1}.

Characterization. Optical absorption spectra were collected using a Shimadzu UV-3600 spectrophotometer. TEM images were obtained using a FEI Technai G2 20 Twin microscope with a LaB_6 filament operated at 200 kV. XRD is performed on a Bruker D8 Discover diffractometer using Cu Kα radiation (λ =1.54 Å). The PLQY was measured in a LabSphere integrating sphere, with excitation provided by monochromatic light selected from a xenon lamp passed through a monochromator (PTI). The emission and excitation spectra were measured with an InGaAs photodiode. The resulting InGaAs signal was amplified using a SRS SR530 lock-in amplifier. XPS data were obtained on a Physical Electronics 5600 photoemission system using monochromatic Al Kα radiation. *J*−*V* curves were acquired in a glovebox with home-built setups. A calibrated filter Si diode (Hamamatsu, S1787-04) served as the reference cell for *J*−*V* measurements.

Conflict of Interest: The authors declare no competing financial interest.

Supporting Information Available: Additional absorption spectra of PbS and PbSe QDs, stability of bromide-terminated PbS QDs, XPS data, growth rate *vs* QD radius under different conditions, and the method used for estimation of size distribution. This material is available free of charge *via* the Internet at http://pubs.acs.org.

Acknowledgment. The authors thank C. L. Perkins for help with XPS measurements. We acknowledge support from the Center for Advanced Solar Photophysics (CASP), an Energy Frontier Research Center funded by the U.S. Department of Energy, Office of Science, Basic Energy Sciences. E.M.M. was supported with an NREL Director's Postdoctoral Fellowship award. DOE funding was provided to NREL through contract DE-AC36-08G028308.

REFERENCES AND NOTES

1. Semonin, O. E.; Luther, J. M.; Choi, S.; Chen, H. Y.; Gao, J. B.; Nozik, A. J.; Beard, M. C. Peak External Photocurrent Quantum Efficiency Exceeding 100% *via* MEG in a Quantum Dot Solar Cell. *Science* **2011**, *334*, 1530–1533.
2. Ip, A. H.; Thon, S. M.; Hoogland, S.; Voznyy, O.; Zhitomirsky, D.; Debnath, R.; Levina, L.; Rollny, L. R.; Carey, G. H.; Fischer, A.; *et al*. Hybrid Passivated Colloidal Quantum Dot Solids. *Nat. Nanotechnol.* **2012**, *7*, 577–582.
3. Gao, J.; Perkins, C. L.; Luther, J. M.; Hanna, M. C.; Chen, H. Y.; Semonin, O. E.; Nozik, A. J.; Ellingson, R. J.; Beard, M. C. *n*-Type Transition Metal Oxide as a Hole Extraction Layer in PbS Quantum Dot Solar Cells. *Nano Lett.* **2011**, *11*, 3263–3266.
4. Luther, J. M.; Law, M.; Beard, M. C.; Song, Q.; Reese, M. O.; Ellingson, R. J.; Nozik, A. J. Schottky Solar Cells Based on Colloidal Nanocrystal Films. *Nano Lett.* **2008**, *8*, 3488–3492.
5. Luther, J. M.; Gao, J. B.; Lloyd, M. T.; Semonin, O. E.; Beard, M. C.; Nozik, A. J. Stability Assessment on a 3% Bilayer PbS/ZnO Quantum Dot Heterojunction Solar Cell. *Adv. Mater.* **2010**, *22*, 3704–3707.
6. Clifford, J. P.; Konstantatos, G.; Johnston, K. W.; Hoogland, S.; Levina, L.; Sargent, E. H. Fast, Sensitive and Spectrally Tuneable Colloidal Quantum-Dot Photodetectors. *Nat. Nanotechnol.* **2009**, *4*, 40–44.
7. Sukhovatkin, V.; Hinds, S.; Brzozowski, L.; Sargent, E. H. Colloidal Quantum-Dot Photodetectors Exploiting Multiexciton Generation. *Science* **2009**, *324*, 1542–1544.
8. Wise, F. W. Lead Salt Quantum Dots: The Limit of Strong Quantum Confinement. *Acc. Chem. Res.* **2000**, *33*, 773–780.
9. Hines, M. A.; Scholes, G. D. Colloidal PbS Nanocrystals with Size-Tunable Near-Infrared Emission: Observation of Post-Synthesis Self-Narrowing of the Particle Size Distribution. *Adv. Mater.* **2003**, *15*, 1844–1849.
10. Yu, W. W.; Falkner, J. C.; Shih, B. S.; Colvin, V. L. Preparation and Characterization of Monodisperse PbSe Semiconductor Nanocrystals in a Noncoordinating Solvent. *Chem. Mater.* **2004**, *16*, 3318–3322.
11. Nozik, A. J.; Beard, M. C.; Luther, J. M.; Law, M.; Ellingson, R. J.; Johnson, J. C. Semiconductor Quantum Dots and Quantum Dot Arrays and Applications of Multiple Exciton Generation to Third-Generation Photovoltaic Solar Cells. *Chem. Rev.* **2010**, *110*, 6873–6890.
12. Beard, M. C.; Luther, J. M.; Semonin, O. E.; Nozik, A. J. Third Generation Photovoltaics based on Multiple Exciton Generation in Quantum Confined Semiconductors. *Acc. Chem. Res.* **2012**, *46*, 1252–1260.
13. Midgett, A. G.; Luther, J. M.; Stewart, J. T.; Smith, D. K.; Padilha, L. A.; Klimov, V. I.; Nozik, A. J.; Beard, M. C. Size and Composition Dependent Multiple Exciton Generation Efficiency in PbS, PbSe, and PbSSe Alloyed Quantum Dots. *Nano Lett.* **2013**, *13*, 3078–3085.
14. Erslev, P. T.; Chen, H.-Y.; Gao, J.; Beard, M. C.; Frank, A. J.; van de Lagemaat, J.; Johnson, J. C.; Luther, J. M. Sharp Exponential Band Tails in Highly Disordered Lead Sulfide Quantum Dot Arrays. *Phys. Rev. B* **2012**, *86*, 155313.
15. Gao, J.; Johnson, J. C. Charge Trapping in Bright and Dark States of Coupled PbS Quantum Dot Films. *ACS Nano* **2012**, *6*, 3292–3303.
16. Luther, J. M.; Law, M.; Song, Q.; Perkins, C. L.; Beard, M. C.; Nozik, A. J. Structural, Optical, and Electrical Properties of Self-Assembled Films of PbSe Nanocrystals Treated with 1,2-Ethanedithiol. *ACS Nano* **2008**, *2*, 271–280.
17. Liu, Y.; Gibbs, M.; Puthussery, J.; Gaik, S.; Ihly, R.; Hillhouse, H. W.; Law, M. Dependence of Carrier Mobility on Nanocrystal Size and Ligand Length in PbSe Nanocrystal Solids. *Nano Lett.* **2010**, *10*, 1960–1969.
18. Evers, W. H.; Goris, B.; Bals, S.; Casavola, M.; de Graaf, J.; van Roij, R.; Dijkstra, M.; Vanmaekelbergh, D. Low-Dimensional Semiconductor Superlattices Formed by Geometric Control over Nanocrystal Attachment. *Nano Lett.* **2013**, *13*, 2317–2323.
19. Choi, J. J.; Bealing, C. R.; Bian, K. F.; Hughes, K. J.; Zhang, W. Y.; Smilgies, D. M.; Hennig, R. G.; Engstrom, J. R.; Hanrath, T. Controlling Nanocrystal Superlattice Symmetry and Shape-Anisotropic Interactions through Variable Ligand Surface Coverage. *J. Am. Chem. Soc.* **2011**, *133*, 3131–3138.
20. Tang, J.; Kemp, K. W.; Hoogland, S.; Jeong, K. S.; Liu, H.; Levina, L.; Furukawa, M.; Wang, X. H.; Debnath, R.; Cha, D. K.; *et al*. Colloidal-Quantum-Dot Photovoltaics Using Atomic-Ligand Passivation. *Nat. Mater.* **2011**, *10*, 765–771.
21. Gao, J.; Jeong, S.; Lin, F.; Erslev, P. T.; Semonin, O. E.; Luther, J. M.; Beard, M. C. Improvement in Carrier Transport Properties by Mild Thermal Annealing of PbS Quantum Dot Solar Cells. *Appl. Phys. Lett.* **2013**, *102*, 043506–5.
22. Bae, W. K.; Joo, J.; Padilha, L. A.; Won, J.; Lee, D. C.; Lin, Q.; Koh, W. K.; Luo, H.; Klimov, V. I.; Pietryga, J. M. Highly Effective Surface Passivation of PbSe Quantum Dots through Reaction with Molecular Chlorine. *J. Am. Chem. Soc.* **2012**, *134*, 20160–20168.
23. Zhitomirsky, D.; Furukawa, M.; Tang, J.; Stadler, P.; Hoogland, S.; Voznyy, O.; Liu, H.; Sargent, E. H. N-Type Colloidal-Quantum-Dot Solids for Photovoltaics. *Adv. Mater.* **2012**, *24*, 6181–6185.

24. Anderson, N. C.; Owen, J. S. Soluble, Chloride-Terminated CdSe Nanocrystals: Ligand Exchange Monitored by ^{1}H and ^{31}P NMR Spectroscopy. *Chem. Mater.* **2013**, *25*, 69–76.
25. Owen, J. S.; Park, J.; Trudeau, P. E.; Alivisatos, A. P. Reaction Chemistry and Ligand Exchange at Cadmium-Selenide Nanocrystal Surfaces. *J. Am. Chem. Soc.* **2008**, *130*, 12279–12281.
26. Zanella, M.; Maserati, L.; Leal, M. P.; Prato, M.; Lavieville, R.; Povia, M.; Krahne, R.; Manna, L. Atomic Ligand Passivation of Colloidal Nanocrystal Films *via* their Reaction with Propyltrichlorosilane. *Chem. Mater.* **2013**, *25*, 1423–1429.
27. Wheeler, L. M.; Neale, N. R.; Chen, T.; Kortshagen, U. R. Hypervalent Surface Interactions for Colloidal Stability and Doping of Silicon Nanocrystals. *Nat. Commun.* **2013**, *4*, 2197.
28. Cademartiri, L.; Bertolotti, J.; Sapienza, R.; Wiersma, D. S.; von Freymann, G.; Ozin, G. A. Multigram Scale, Solventless, and Diffusion-Controlled Route to Highly Monodisperse PbS Nanocrystals. *J. Phys. Chem. B* **2006**, *110*, 671–673.
29. Moreels, I.; Lambert, K.; Smeets, D.; De Muynck, D.; Nollet, T.; Martins, J. C.; Vanhaecke, F.; Vantomme, A.; Delerue, C.; Allan, G.; *et al.* Size-Dependent Optical Properties of Colloidal PbS Quantum Dots. *ACS Nano* **2009**, *3*, 3023–3030.
30. Moreels, I.; Justo, Y.; De Geyter, B.; Haustraete, K.; Martins, J. C.; Hens, Z. Size-Tunable, Bright, and Stable PbS Quantum Dots: A Surface Chemistry Study. *ACS Nano* **2011**, *5*, 2004–2012.
31. Dilena, E.; Xie, Y.; Brescia, R.; Prato, M.; Maserati, L.; Krahne, R.; Paolella, A.; Bertoni, G.; Povia, M.; Moreels, I.; Manna, L. CuInxGa1−xS2 Nanocrystals with Tunable Composition and Band Gap Synthesized *via* a Phosphine-Free and Scalable Procedure. *Chem. Mater.* **2013**, *25*, 3180–3187.
32. Kovalenko, M. V.; Talapin, D. V.; Loi, M. A.; Cordella, F.; Hesser, G.; Bodnarchuk, M. I.; Heiss, W. Quasi-Seeded Growth of Ligand-Tailored PbSe Nanocrystals through Cation-Exchange-Mediated Nucleation. *Angew. Chem., Int. Ed.* **2008**, *47*, 3029–3033.
33. Talapin, D. V.; Rogach, A. L.; Haase, M.; Weller, H. Evolution of an Ensemble of Nanoparticles in a Colloidal Solution: Theoretical Study. *J. Phys. Chem. B* **2001**, *105*, 12278–12285.
34. Peng, X.; Wickham, J.; Alivisatos, A. P. Kinetics of II-VI and III-V Colloidal Semiconductor Nanocrystal Growth: 'Focusing' of Size Distributions. *J. Am. Chem. Soc.* **1998**, *120*, 5343–5344.
35. Seeton, C. J. Viscosity-Temperature Correlation for Liquids. *Tribol. Lett.* **2006**, *22*, 67–78.
36. Lifshitz, I. M.; Slyozov, V. V. The Kinetics of Precipitation from Supersaturated Solid Solutions. *J. Phys. Chem. Solids* **1961**, *19*, 35–50.
37. Dai, Q.; Wang, Y.; Zhang, Y.; Li, X.; Li, R.; Zou, B.; Seo, J.; Wang, Y.; Liu, M.; Yu, W. W. Stability Study of PbSe Semiconductor Nanocrystals over Concentration, Size, Atmosphere, and Light Exposure. *Langmuir* **2009**, *25*, 12320–12324.
38. Gao, J.; Luther, J. M.; Semonin, O. E.; Ellingson, R. J.; Nozik, A. J.; Beard, M. C. Quantum Dot Size Dependent J-V Characteristics in Heterojunction ZnO/PbS Quantum Dot Solar Cells. *Nano Lett.* **2011**, *11*, 1002–1008.